ACS SENSORS

pubs.acs.org/acssensors

Article

Electrochemiluminescence Biosensor for Hyaluronidase Based on the Adjustable Electrostatic Interaction between the Surface-Charge-Controllable Nanoparticles and Negatively Charged Electrode

Zhixin Li, Xiaoli Huang, Hongning Liu,* Fang Luo, Bin Qiu, Zhenyu Lin,* and Huixing Chen*

Cite This: *ACS Sens.* 2022, 7, 2012−2019

Read Online

ACCESS | Metrics & More | Article Recommendations | Supporting Information

ABSTRACT: A novel electrochemiluminescence (ECL) biosensor for hyaluronidase (HAase) based on the adjustable electrostatic interaction between the surface-charge-controllable nanoparticles and negatively charged electrode has been devised. Hyaluronic acid (HA)-coated amino-modified ruthenium bipyridine-doped silica nanoparticles ($Ru@SiO_2-NH_2@HA$ NPs) have been synthesized and act as ECL indicators, and the surface of this particle is negatively charged because HA contains a large amount of OH− and COO−. The strong electrostatic repulsion between the $Ru@SiO_2-NH_2@HA$ NPs and negatively charged indium tin oxide (ITO) electrode surface leads to the detection of a low-intensity ECL signal. In the presence of HAase, the HA on the surface of the $Ru@SiO_2-NH_2@HA$ NPs can be decomposed, and the particles can be transformed into positively charged amino-modified ruthenium bipyridine-doped silica nanoparticles ($Ru@SiO_2-NH_2$ NPs), which can be concentrated near the surface of the ITO electrode through electrostatic attraction, and result in the detection of an enhanced ECL signal. The ECL of the system has a good linear relationship with HAase concentration in the range of 2.0−60 U/mL, and the limit of detection was 0.37 U/mL. The designed biosensor had been applied to detect the target in real samples with satisfied results.

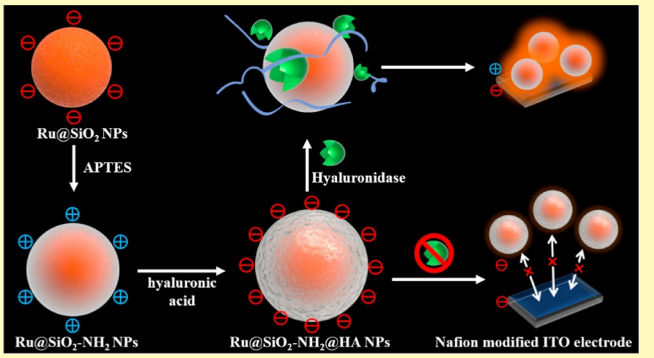

KEYWORDS: *electrochemiluminescence, hyaluronidase, hyaluronic acid, surface-charge-controllable nanoparticle, electrostatic interaction, negatively charged electrode*

Surface-charge-controllable nanoparticles have been applied in the construction of biosensors frequently.[1] For example, Ren et al. used gold nanoparticles (AuNPs) modified with the target substrate peptide as the signal probe to detect protein tyrosine (Tyr) kinase.[2] The substrate peptide modified on the surface of AuNPs can be phosphorylated by the target, which makes the negative charge on the surface of AuNPs increase significantly and results in the change in zeta potential. The colorimetric sensor based on surface-charge-controllable nanoparticles had been reported.[3] Positively charged AuNPs were coated by DNA/RNA oligonucleotide aptamers so that AuNPs can remain dispersed in the solution through electrostatic repulsion. When the target is combined with the aptamer, the negative charge on the surface of AuNPs becomes weaker and the positive charge is strengthened, leading to the aggregation of AuNPs and causing a color change in the system. However, until now, nearly no electrochemiluminescence (ECL) sensor has been constructed by regulating the surface charge of nanoparticles.

The difference in electrostatic interaction between signal probes with different charges and a charged working electrode can affect the opportunity of signal probes reaching the electrode interface, thereby influencing the detection of electrochemical or ECL signals.[4] This characteristic had been applied to design biosensors for diverse targets.[5] However, most of these biosensors are realized through the regulation of the length of DNAs by the targets and hence affect the number of negative charges labeled on the probes, and it cannot be used for the detection of the target that cannot influence the DNA strands' length. Furthermore, most of them are realized by the change in electrostatic repulsive force, and nearly no

Received: April 13, 2022
Accepted: June 13, 2022
Published: June 22, 2022

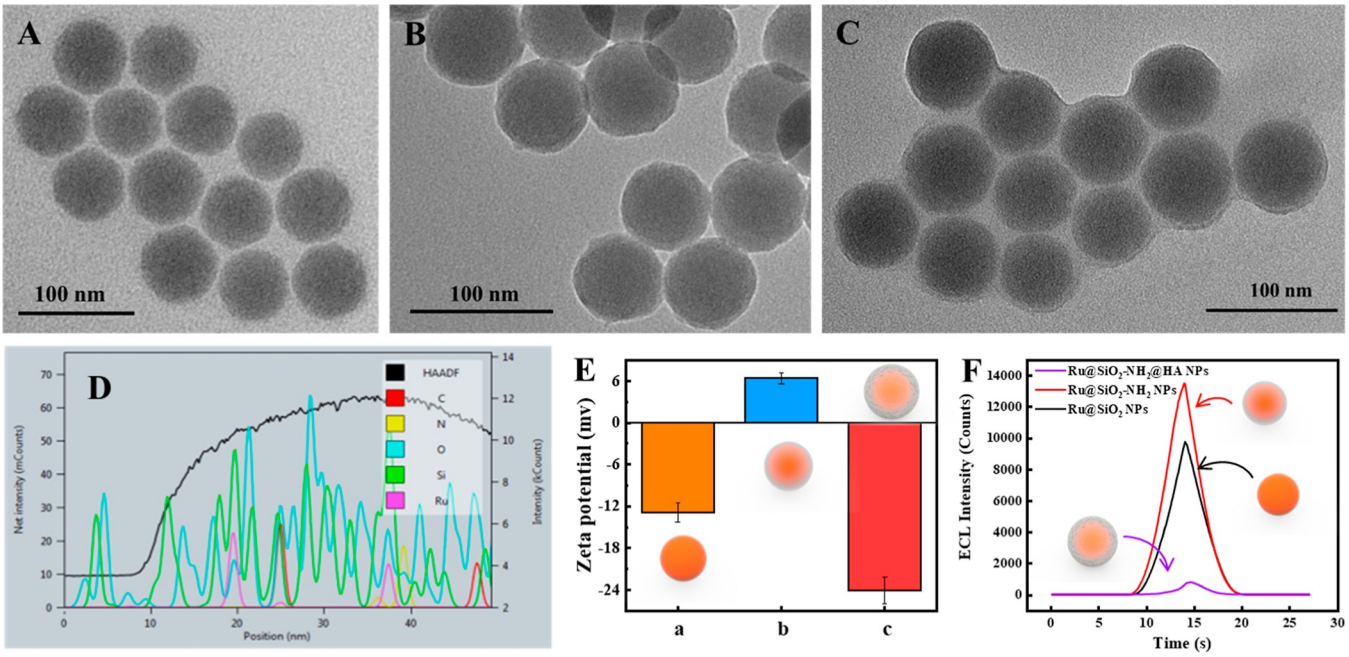

Figure 1. TEM image of (A) $Ru@SiO_2$ NPs, (B) $Ru@SiO_2{-}NH_2$ NPs, and (C) $Ru@SiO_2{-}NH_2$@HA NPs; (D) EDS image of $Ru@SiO_2{-}NH_2$@HA NPs; (E) zeta potential of (a) $Ru@SiO_2$ NPs, (b) $Ru@SiO_2{-}NH_2$ NPs, and (c) $Ru@SiO_2{-}NH_2$@HA NPs; (F) ECL intensity produced from $Ru@SiO_2$ NPs, $Ru@SiO_2{-}NH_2$ NPs, and $Ru@SiO_2{-}NH_2$@HA NPs.

attention had been paid to design biosensors which can change the direction of the electrostatic interaction.

Hyaluronidase (HAase) is an enzyme which can hydrolyze hyaluronic acid (HA) with high efficiency.[6] Excessive HAase has been reported to be relevant to some malignancies at the early stages,[7] so it can work as a tumor biomarker.[8] Hence, measuring HAase through a high-accuracy method is essential. Many methods, including fluorescent methods,[9−11] colorimetric methods,[12] weighting methods,[13] and so on,[14] have been reported for the HAase quantification so far. Our group has developed two ECL methods for HAase detection based on changing the molecular weight of signal probes by HAase for signal probe ultrafiltration and collection[15] and decomposing the hydrogel loaded with signal probes by HAase for signal probe release.[16] However, the efficiency of these ECL methods was low, and a long reaction time is needed. Hence, efforts need to be made on addressing the abovementioned problems.

In this work, a novel ECL method based on adjustable electrostatic interaction between the surface-charge-controllable nanoparticles and negatively charged electrode had been proposed. The HA-coated amino-modified ruthenium bipyridine-doped silica nanoparticles ($Ru@SiO_2{-}NH_2$@HA NPs) with a lot of negative charges have been synthesized as the charge-controllable ECL nanoprobes. As the core of nanoprobes, $Ru@SiO_2$ NPs with a porous structure, which allowed the small molecules to pass through the pore of the nanoparticle to exchange the electron and energy, have been widely used in ECL biosensor construction.[17] The electrostatic repulsion between the $Ru@SiO_2{-}NH_2$@HA NPs and the negatively charged indium tin oxide (ITO) electrode surface leads to the detection of a low-intensity ECL signal. When HAase exists, the HA on the surface of the $Ru@SiO_2{-}NH_2$@HA NPs can be decomposed, and therefore, the $Ru@SiO_2{-}NH_2$@HA NPs with a lot of negative charges can be transformed into amino-modified ruthenium bipyridine-doped silica nanoparticles ($Ru@SiO_2{-}NH_2$ NPs) with a lot of positive charges. $Ru@SiO_2{-}NH_2$ NPs can be concentrated near the surface of the ITO electrode through electrostatic attraction and result in the detection of an enhanced ECL signal, which can be recorded and used for HAase activity characterization.

EXPERIMENTAL SECTION

Reagents and Apparatus. Manufacturers and suppliers of all experimental reagents and apparatus mentioned in the manuscript are detailed in the Supporting Information.

Synthesis of $Ru@SiO_2{-}NH_2$ NPs. Ruthenium bipyridine-doped silica nanoparticles ($Ru@SiO_2$ NPs) were obtained based on our early reported synthesis method[16] and dispersed in anhydrous ethanol (10 mg/mL) for later use. Then, 50 μL of 3-aminopropyltriethoxysilane (APTES, 0.2%) and 1.2 mL of the abovementioned $Ru@SiO_2$ NPs solution were added in 4.75 mL of anhydrous ethanol and incubated for 2 h. After that, the resulting solution was centrifuged (7000 r/min, 10 min) and then washed with anhydrous ethanol and ultrapure water three times to purify $Ru@SiO_2{-}NH_2$ NPs. The resulting $Ru@SiO_2{-}NH_2$ NPs were dissolved in ultrapure water (4 mg/mL) for later use.

Synthesis of $Ru@SiO_2{-}NH_2$@HA NPs. HA sodium salt solution (1.8 mL, 0.1%) was blended with 200 μL of 1-(3-dimethylaminopropyl)-3-ethylcarbodiimide hydrochloride and 200 μL of *N*-hydroxy succinimide and incubated for 15 min to activate carboxyl, and then, 1.5 mL of the proposed $Ru@SiO_2{-}NH_2$ NP solution was dripped into the abovementioned mixed solution slowly and reacted with HA for 12 h. Next, the resulting solution was centrifuged (7000 r/min, 10 min) and washed with ultrapure water three times and finally dissolved in ultrapure water (4 mg/mL) for later use. After that, the $Ru@SiO_2{-}NH_2$@HA NP solution was obtained as the surface-charge-controllable ECL indicator in this study.

Procedures for HAase Detection. As the ECL signal probe, the resulting $Ru@SiO_2{-}NH_2$@HA NP solution (100 μL) mixed with 100 μL of deionized water was dripped into different concentrations of HAase solution [400 μL, containing 15 mM phosphate-buffered saline (PBS)] and incubated at 37 °C for 1 h. Then, the proposed mixed solution was added in PBS (1.6 mL, 10 mM) containing 8 μL of tripropylamine. In the detection procedure, the scan rate of the electrochemical workstation was 100 mV/s, and the scanning

https://doi.org/10.1021/acssensors.2c00801
ACS Sens. 2022, 7, 2012−2019

Scheme 1. Principle of the Homogeneous ECL Biosensor for HAase Detection Based on the Adjustable Electrostatic Interaction between the Surface-Charge-Controllable Nanoparticles and Negatively Charged Electrode, Including the (a) Construction of Surface-Charge-Controllable Nanoparticles and the (b) Detection Process of HAase

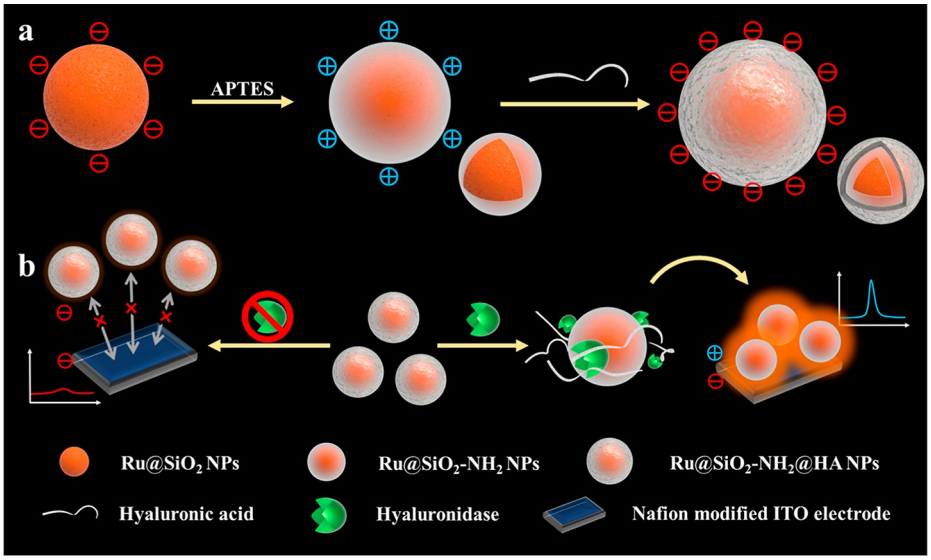

potential range was from 0.6 to 1.6 V; the photomultiplier tube voltage of the ultraweak luminescence analyzer was −800 V. The ECL signal produced from the abovementioned solution was recorded, and the procedure was repeated three times.

Preparation of the Interfering Substance Sample. The concentration of NaCl, KCl, $MgCl_2$, $CaCl_2$, and urea solution was 10 mM; the concentration of glucose (Glu) and uric acid (UA) was 100 nM; the concentration of glutathione (GSH) and human serum albumin (HAS) was 10 nM; and the concentration of Tyr was 100 U/mL. The final concentration of PBS in each interfering substance solutions was 15 mM.

Preparation of Real Samples. The urine samples including healthy people and patients analyzed in this work was obtained from the Affiliated Hospital of Putian University. The urine samples were centrifuged (8000 r/min) for 5 min, and the supernatant (400 μL) was mixed with 100 μL of PBS (60 mM) and Ru@SiO_2−NH_2@HA NP solution (100 μL) and then incubated at 37 °C for 1 h. After that, the abovementioned mixed solution can be obtained for detection.

RESULTS AND DISCUSSION

Characterization of Prepared Nanoparticles. The characterization of Ru@SiO_2 NPs, Ru@SiO_2−NH_2 NPs, and Ru@SiO_2−NH_2@HA NPs was first performed. The TEM images of Ru@SiO_2 NPs, Ru@SiO_2−NH_2 NPs, and Ru@SiO_2−NH_2@HA NPs are shown in Figure 1A−C, respectively. The results indicated that Ru@SiO_2 NPs, Ru@SiO_2−NH_2 NPs, and Ru@SiO_2−NH_2@HA NPs with uniform size have been synthesized. High-resolution TEM of Ru@SiO_2 NPs is shown in Figure S1 (Supporting Information), demonstrating the porous structure of Ru@SiO_2 NPs, which allowed the small molecules to pass through to exchange the electron and energy during the ECL process. In addition, energy-dispersive spectrometry (EDS) of Ru@SiO_2−NH_2@HA NPs (Figure 1D) proved the successful modification of APTES and HA.

The zeta potential of Ru@SiO_2 NPs, Ru@SiO_2−NH_2 NPs, and Ru@SiO_2−NH_2@HA NPs was −12.87, 6.42, and −24.06 mV, respectively (Figure 1E), indicating that the difference in the surface charge of the prepared nanoparticles is related to the different groups modified on their surface. The negative charge on the surface of Ru@SiO_2 NPs in solution is caused by the $SiOH/SiO^-$ on their surface; the positive charge on the surface of Ru@SiO_2−NH_2 NPs is caused by NH_2/NH_3^+ modified on their surface through APTES; the negative charge on the surface of Ru@SiO_2−NH_2@HA NPs in solution is caused by a large number of OH/O^- and $COOH/COO^-$ coated on their surface through HA modification.

As depicted in Figure 1F, the ECL signal produced by Ru@SiO_2−NH_2 NPs was higher than that from Ru@SiO_2 NPs, indicating that positively charged Ru@SiO_2−NH_2 NPs can be concentrated near the surface of the negatively charged ITO electrode easily through the effect of electrostatic attraction and produce an enhanced ECL signal, thereby promoting the ECL efficiency. The ECL signal produced from Ru@SiO_2−NH_2@HA NPs was especially weak; the reason lies in the fact that this nanoparticle is negatively charged, and the electrostatic repulsion keeps Ru@SiO_2−NH_2@HA NPs away from the surface of the negatively charged ITO electrode.

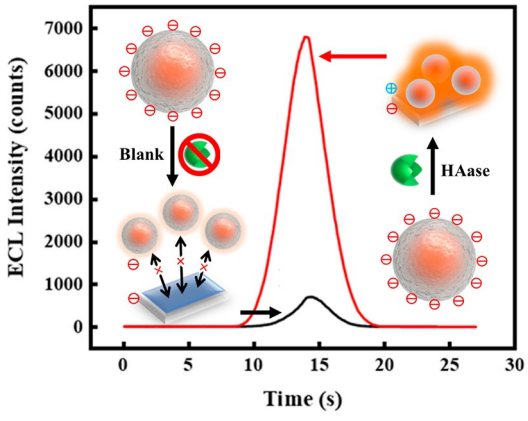

Figure 2. Feasibility test of the ECL biosensor.

Principle and Feasibility of the Proposed ECL Biosensor for HAase. Scheme 1 shows the principle of the developed biosensor. Ru@SiO_2 NPs carrying plenty of silicon hydroxyls were modified by APTES and transformed into Ru@SiO_2−NH_2 NPs. Compared with Ru@SiO_2 NPs, the Ru@

https://doi.org/10.1021/acssensors.2c00801
ACS Sens. 2022, 7, 2012−2019

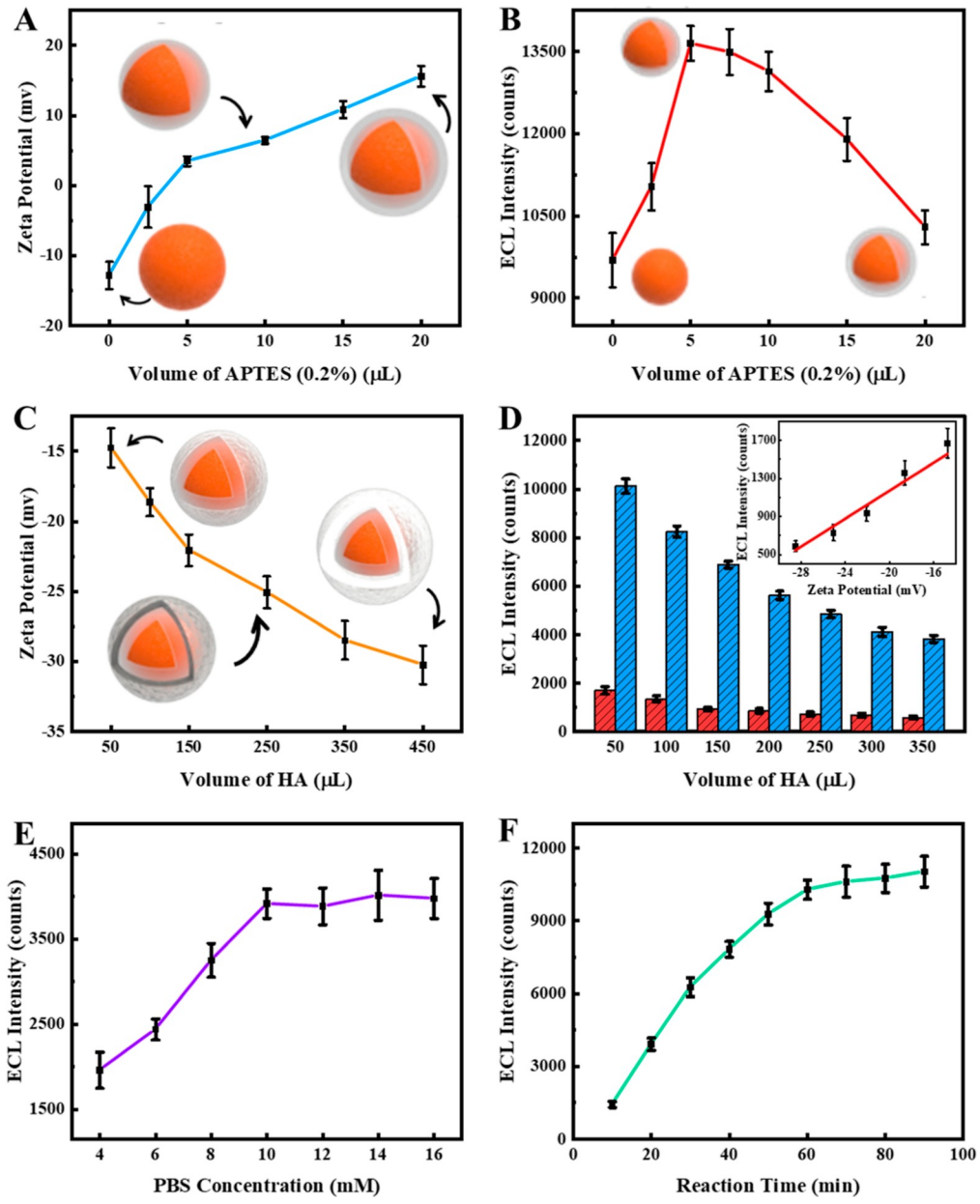

Figure 3. Effect of volumes of 0.2% APTES used on (A) zeta potential of Ru@SiO_2−NH_2 NPs and (B) ECL signal recorded; (C) effect of volumes of HA on the zeta potential of Ru@SiO_2−NH_2@HA NPs; (D) difference of ECL signals recorded between the control and experimental groups under different volumes of HA. The inset shows the linear relationship between the ECL recorded and the zeta potential of Ru@SiO_2−NH_2@HA NPs; (E) effect of ionic strength (PBS concentration) on ECL intensity; (F) effect of enzymolysis reaction time on ECL intensity.

SiO_2−NH_2 NPs which contain plenty of amidogens and positive charges can be concentrated near the negatively charged ITO electrode through electrostatic attraction. Then, Ru@SiO_2−NH_2 NPs were coated by HA through amido bonds and transformed into Ru@SiO_2−NH_2@HA NPs which contain a lot of negative charges, and this nanoparticle has been used as the ECL-reporting probe. In the absence of HAase, the strong electrostatic repulsion occurred between negatively charged Ru@SiO_2−NH_2@HA NPs and the negatively charged ITO electrode surface, so only the low ECL signal is produced. When HAase exists, the HA coated on the Ru@SiO_2−NH_2@HA NPs can be decomposed, which results in the decrease in the negative charges on the surface of Ru@SiO_2−NH_2@HA NPs, and even make Ru@SiO_2−NH_2@HA NPs transform into positively charged Ru@SiO_2−NH_2 NPs. Ru@SiO_2−NH_2 NPs can be concentrated near the surface of the ITO electrode through electrostatic attraction and result in an enhanced ECL signal being produced. The ECL response of the system has some relationship with HAase concentration, which can be used for quantitative detection.

The feasibility was verified by a simple control trial. As shown in Figure 2, a weak ECL signal was recorded when HAase did not exist. However, a strong ECL signal was detected after the addition of HAase. These results verify the principle of the abovementioned presumption.

Optimization of the Reaction Conditions. The surface charge is an important factor of the proposed biosensor. Modification of amino can observably improve electrostatic attraction between Ru@SiO_2−NH_2 NPs and the negatively charged ITO electrode, and the enhanced ECL signal can be

https://doi.org/10.1021/acssensors.2c00801
ACS Sens. 2022, 7, 2012−2019

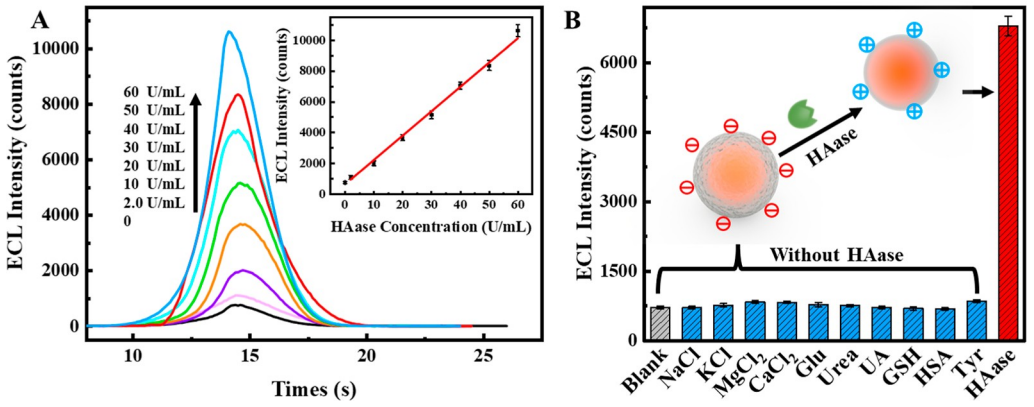

Figure 4. (A) ECL signal produced from the homogeneous ECL biosensor and different concentrations of HAase. The inset shows the linear relationship between the concentration of Haase and ECL intensity; (B) selectivity of the proposed biosensor. The concentration of NaCl, KCl, $MgCl_2$, $CaCl_2$, and urea solution was 10 mM; the concentration of Glu and UA was 100 nM; the concentration of GSH and HAS was 10 nM; and the concentration of Tyr was 100 U/mL.

Table 1. Comparison of Different Strategies for HAase Quantification

method	linear range (U/mL)	LOD (U/mL)	detection time (min)	refs
fluorescence	1.25−50	0.625	180	18
fluorescence	0.1−80	0.06	120	19
fluorescence	1−50	0.7	45	20
fluorescence	0.025−0.2	0.007	90	21
fluorescence	0.1−8	0.05	96	10
ECL	2.0−40	0.33	150	15
fluorescence	0.05−2 and 2.75−5	0.02	100	22
fluorescence	0.5−37.5	0.30	65	11
ECL	2.0−60	0.37	60	this work

detected. However, excess modification of APTES may reduce the hydrophilicity of $Ru@SiO_2-NH_2$ NPs and hence cause a low ECL efficiency. Therefore, the dosage of APTES used in the process of $Ru@SiO_2-NH_2$ NP synthesis was optimized. The zeta potential increased with the increase in APTES volume (Figure 3A), indicating that the charges on the surface of $Ru@SiO_2-NH_2$ NPs are controllable. Figure 3B shows that the ECL intensity of the system increased first with the increase in APTES volume and reached a peak at 5 μL, indicating that 5 μL is the optimized dosage of APTES. When the volume of APTES exceeded 5 μL, the ECL intensity was decreased and the precipitation was observed, and the reason lies in the fact that excess modification reduces the hydrophilicity of $Ru@SiO_2-NH_2$ NPs, thus leading to coagulation.

The effect of the amount of HA coated on the surface of $Ru@SiO_2-NH_2@HA$ NPs had been studied. A small amount of HA modified on $Ru@SiO_2-NH_2$ NPs cannot increase the amounts of negative charges on the nanoparticles effectively, hence leading to a high background signal. In contrast, a large amount of HA modified on $Ru@SiO_2-NH_2$ NPs can produce a low background signal but reduce the sensitivity of the proposed biosensor. Therefore, an appropriate dosage of HA for high signal to background ratio biosensor fabrication is needed. As shown in Figure 3C, the zeta potential decreased with the increase in HA volume, indicating that the negative charges on the surface of $Ru@SiO_2-NH_2@HA$ NPs can be

Table 2. Determination of HAase Concentration in Urine Samples Using the Homogeneous ECL Strategy Based on the Surface-Charge-Controllable Strategy and ELISA Kit (n = 3)

urine samples	spiked (U/mL)		detected HAase by the ECL method (U/mL)	RSD (%)	detected HAase by ELISA (U/mL)	recovery rate (%)
healthy people	1	0	3.15	3.53	3.22	
		5.0	7.99	1.56	8.26	96.72
		10.0	13.20	2.13	13.20	100.46
		15.0	18.81	2.38	18.17	104.42
	2	0	2.05	2.97	2.16	
		5.0	7.00	5.26	7.21	99.13
		10.0	12.35	2.20	12.19	102.98
		15.0	17.40	4.18	17.25	102.35
	3	0	2.50	4.63	2.38	
		5.0	7.56	1.17	7.44	101.30
		10.0	12.59	2.20	12.42	100.97
		15.0	18.00	3.95	17.49	103.35
patients	1	0	41.55	2.38	41.82	
		5.0	46.37	3.00	46.93	96.32
		10.0	51.74	2.44	51.79	101.90
		15.0	56.25	3.45	56.88	97.99
	2	0	39.51	1.51	39.62	
		5.0	44.39	3.50	44.69	97.60
		10.0	49.43	2.30	49.76	99.17
		15.0	54.67	2.83	54.80	101.07
	3	0	36.86	2.51	37.07	
		5.0	42.02	4.89	42.20	103.11
		10.0	47.38	4.21	47.24	105.20
		15.0	52.24	6.39	51.96	102.49

controlled by HA dosage. As depicted in Figure 3D, the ECL signal produced from $Ru@SiO_2-NH_2@HA$ NPs decreased with the increase in HA solution (0.1 mg/mL) volume in both the control and the experimental groups. The signal to background ratio is the best at 150 μL of HA, which had been chosen in the following study.

The inset in Figure 3D shows that the ECL intensity has a good linear relationship with the zeta potential of the nanoparticles, and the linear equation was I_{ECL}/counts = 73.39 Z/mV + 2635.59, where I_{ECL} and Z represent the ECL

https://doi.org/10.1021/acssensors.2c00801
ACS Sens. 2022, 7, 2012−2019

intensity of Ru@SiO_2−NH_2@HA NPs and the zeta potential of Ru@SiO_2−NH_2@HA NPs, respectively. The correlation coefficient is 0.974, demonstrating a close relationship between the ECL intensity and surface charge of Ru@SiO_2−NH_2@HA NPs.

The ionic strength used in detection solution has been optimized. Theoretically, the weak ionic strength in the solution favors the electrostatic adsorption between electrodes and nanoparticles but may reduce the electron transfer efficiency during the ECL process. As shown in Figure 3E, the ECL intensity of the system increased with the concentration of PBS and stabilized after the concentration of PBS reached 10 mM, indicating that the ECL intensity is mainly affected by the electron transfer efficiency. A weak ionic strength can lead to the electron transfer efficiency reduction, and a sufficient ionic strength can saturate the number of ions on the surface of nanoparticles and the electrode to provide a stable electron transfer efficiency. Finally, 10 mM PBS had been chosen in the following study.

The reaction time of HAase and Ru@SiO_2−NH_2@HA NPs is also an important condition that needs to be optimized. As shown in Figure 3F, with the increase in reaction time, the ECL intensity increased first and then reached a platform at 60 min (the standard sample containing 60 U/mL HAase), indicating that 60 min is the optimized reaction time.

Performance of the Proposed System. Figure 4A shows that the ECL response was recorded after the addition of different HAase concentrations under optimized conditions, and the inset shows a good linear relationship between the ECL signal detected and the HAase concentration in the range of 2.0−60 U/mL. The linear equation was

$$I_{ECL}/\text{counts} = 158.02C_{HAase}/(\text{U/mL}) + 624.22,$$
$$R = 0.9974$$

where C_{HAase} and I_{ECL} represent the HAase concentration of the sample and the ECL intensity, respectively. R is the correlation coefficient. The limit of detection (LOD) is 0.37 U/mL (S/N = 3).

As shown in Table 1, compared with most of the other methods, the current method has a wide linear range and sufficient sensitivity for HAase detection. Compared with our early reported ECL strategy,[16] the proposed strategy not only improves the efficiency of enzymatic hydrolysis and shortens the detection time but also improves the ECL efficiency of the sensor in homogeneous solution using electrostatic interaction to aggregate ECL signal probes near the surface of the working electrode.

The selectivity of the proposed ECL strategy is shown in Figure 4B. Only weak ECL signals were recorded on the blank group or in the presence of interfering substances, while a strong ECL signal was recorded in the presence of a target, demonstrating the high selectivity of the proposed biosensor. Ru@SiO_2−NH_2@HA NPs had been stored at 4 °C and had been used for HAase detection every week. The outcomes showed that there was no significant difference between the Ru@SiO_2−NH_2@HA NPs after 4 weeks of storage and the recently prepared Ru@SiO_2−NH_2@HA NPs, demonstrating the good stability of Ru@SiO_2−NH_2@HA NPs.

Application of the Proposed Biosensor. HAase in urine provided from healthy volunteers and cancer patients was quantified by the proposed ECL biosensor, and standard addition recovery rates were obtained to evaluate the performance of the proposed method. In addition, the proposed ECL biosensor was compared with the ELISA method for further verifying the accuracy of the method. As depicted in Table 2, the concentration of HAase in the urine of patients was much higher than that in the urine of healthy people. The standard addition recovery rates were in the range of 96.32−105.2%, and the relative standard deviations (RSDs) were not over 6.4%. Furthermore, the detection result of the proposed method was similar to that of the ELISA method. All these outcomes demonstrate the effectiveness and reliability of the proposed ECL biosensor.

CONCLUSIONS

In conclusion, a novel ECL biosensor based on the adjustable electrostatic interaction between the surface-charge-controllable nanoparticles and negatively charged electrode has been devised for HAase quantification. It is the first report, the ECL strategy based on the target triggers changes in the surface charge of ECL nanoprobes, which in turn causes the change in the electrostatic interaction between the nanoparticles and the negatively charged ITO electrode. This strategy can realize target detection through the regulation of the surface charge, thereby improving the efficiency of homogeneous ECL sensing and expanding the applications of ECL detection. The designed biosensor has high selectivity and sensitivity, which had been applied to detect the target in real samples with satisfied results.

ASSOCIATED CONTENT

Supporting Information

The Supporting Information is available free of charge at https://pubs.acs.org/doi/10.1021/acssensors.2c00801.

Materials and apparatus used in this work (PDF)

AUTHOR INFORMATION

Corresponding Authors

Hongning Liu − *Institute for Advanced Study, Research Center for Differentiation and Development of TCM Basic Theory, Jiangxi University of Chinese Medicine, Nanchang 330004 Jiangxi, China*; Email: 19820002@jxutcm.edu.cn

Zhenyu Lin − *Ministry of Education Key Laboratory for Analytical Science of Food Safety and Biology, Fujian Provincial Key Laboratory of Analysis and Detection for Food Safety, College of Chemistry, Fuzhou University, Fuzhou 350116 Fujian, China*; orcid.org/0000-0001-7890-6812; Email: zylin@fzu.edu.cn

Huixing Chen − *Department of Hepatobiliary Surgery and Fujian Institute of Hepatobiliary Surgery, Fujian Medical University Union Hospital, Fujian Medical University Cancer Center, Fuzhou 350000 Fujian, China*; Email: chenhuixing@163.com

Authors

Zhixin Li − *Institute for Advanced Study, Research Center for Differentiation and Development of TCM Basic Theory, Jiangxi University of Chinese Medicine, Nanchang 330004 Jiangxi, China; Ministry of Education Key Laboratory for Analytical Science of Food Safety and Biology, Fujian Provincial Key Laboratory of Analysis and Detection for Food Safety, College of Chemistry, Fuzhou University, Fuzhou 350116 Fujian, China*

https://doi.org/10.1021/acssensors.2c00801
ACS Sens. 2022, 7, 2012−2019

Xiaoli Huang − *Department of Obstetrics and Gynecology, The First Affiliated Hospital of Fujian Medical University, Fujian Medical University, Fuzhou 350001 Fujian, China*

Fang Luo − *Ministry of Education Key Laboratory for Analytical Science of Food Safety and Biology, Fujian Provincial Key Laboratory of Analysis and Detection for Food Safety, College of Chemistry, Fuzhou University, Fuzhou 350116 Fujian, China*

Bin Qiu − *Ministry of Education Key Laboratory for Analytical Science of Food Safety and Biology, Fujian Provincial Key Laboratory of Analysis and Detection for Food Safety, College of Chemistry, Fuzhou University, Fuzhou 350116 Fujian, China*

Complete contact information is available at: https://pubs.acs.org/10.1021/acssensors.2c00801

Author Contributions

Z.L. and X.H. contributed equally to this work. Z. X. L., H. X. C., and Z. Y. L. conceived and designed the study; Z. X. L. and X. L. H. conducted the experiments; Z. X. L., H. N. L., J. W., F. L., B. Q., and Z. Y. L. analyzed the data; Z. X. L., H. N. L., and Z. Y. L. wrote the paper. All authors discussed the data and the results. All authors have given approval to the final version of the manuscript.

Notes

The authors declare no competing financial interest.

■ ACKNOWLEDGMENTS

This project was financially supported by the National Sciences Foundation of China (22174018) and the Sciences Foundation of Fujian Province (2020J011007).

■ REFERENCES

(1) (a) Chen, L.; Xu, S.; Li, W.; Ren, T.; Yuan, L.; Zhang, S.; Zhang, X.-B. Tumor-acidity activated surface charge conversion of two-photon fluorescent nanoprobe for enhanced cellular uptake and targeted imaging of intracellular hydrogen peroxide. *Chem. Sci.* **2019**, *10*, 9351−9357. (b) Lee, G.-Y.; Bong, J.-H.; Kim, J. Y.; Yoo, G.; Park, M.; Kang, M.-J.; Jose, J.; Pyun, J.-C. Thermophoretic diagnosis of autoimmune diseases based on Escherichia coli with autodisplayed autoantigens. *Anal. Chim. Acta* **2019**, *1055*, 106−114. (c) Li, L.; Wang, Z.; Lu, Y.; Zhu, K.; Zong, S.; Cui, Y. DNA-assisted synthesis of Ortho-NanoDimer with sub-nanoscale controllable gap for SERS application. *Biosens. Bioelectron.* **2021**, *172*, 112769.

(2) Yi, F.; Huang, X.; Ren, J. Simple and Sensitive Method for Determination of Protein Kinase Activity Based on Surface Charge Change of Peptide-Modified Gold Nanoparticles As Substrates. *Anal. Chem.* **2018**, *90*, 3871−3877.

(3) (a) Luo, F.; Zheng, L.; Chen, S.; Cai, Q.; Lin, Z.; Qiu, B.; Chen, G. An aptamer-based fluorescence biosensor for multiplex detection using unmodified gold nanoparticles. *Chem. Commun.* **2012**, *48*, 6387−6389. (b) Sun, S.; Li, L.; Wu, X.; Tang, R.; Lei, C.; Wang, H.-H.; Huang, Y.; Nie, Z.; Yao, S. Dual-Product Synergistically Enhanced Colorimetric Assay for Sensitive Detection of Lipid Transferase Activity. *Anal. Chem.* **2020**, *92*, 15236−15243.

(4) (a) Luo, X.; Lee, T. M.-H.; Hsing, I.-M. Immobilization-Free Sequence-Specific Electrochemical Detection of DNA Using Ferrocene-Labeled Peptide Nucleic Acid. *Anal. Chem.* **2008**, *80*, 7341−7346. (c) Xuan, F.; Luo, X.; Hsing, I.-M. Sensitive immobilization-free electrochemical DNA sensor based on isothermal circular strand displacement polymerization reaction. *Biosens. Bioelectron.* **2012**, *35*, 230−234. (d) Ni, J.; Lin, H.; Yang, W.; Liao, Y.; Wang, Q.; Luo, F.; Guo, L.; Qiu, B.; Lin, Z. Homogeneous Electrochemiluminescence Biosensor for the Detection of RNase A Activity and Its Inhibitor. *Anal. Chem.* **2019**, *91*, 14751−14756. (e) Li, D.; Li, Y.; Luo, F.; Qiu, B.; Lin, Z. Ultrasensitive Homogeneous Electrochemiluminescence Biosensor for a Transcription Factor Based on Target-Modulated Proximity Hybridization and Exonuclease III-Powered Recycling Amplification. *Anal. Chem.* **2020**, *92*, 12686−12692.

(5) (a) Xuan, F.; Fan, T. W.; Hsing, I.-M. Electrochemical Interrogation of Kinetically-Controlled Dendritic DNA/PNA Assembly for Immobilization-Free and Enzyme-Free Nucleic Acids Sensing. *ACS Nano* **2015**, *9*, 5027−5033. (b) Hou, T.; Xu, N.; Wang, W.; Ge, L.; Li, F. Truly Immobilization-Free Diffusivity-Mediated Photoelectrochemical Biosensing Strategy for Facile and Highly Sensitive MicroRNA Assay. *Anal. Chem.* **2018**, *90*, 9591−9597. (c) Lu, F.; Yang, L.; Hou, T.; Li, F. Label-free and ″signal-on″ homogeneous photoelectrochemical cytosensing strategy for ultrasensitive cancer cell detection. *Chem. Commun.* **2020**, *56*, 11126−11129.

(6) Stern, R.; Jedrzejas, M. J. Hyaluronidases: Their Genomics, Structures, and Mechanisms of Action. *Chem. Rev.* **2006**, *106*, 818−839.

(7) (a) West, D. C.; Hampson, I. N.; Arnold, F.; Kumar, S. Angiogenesis Induced by Degradation Products of Hyaluronic Acid. *Science* **1985**, *228*, 1324−1326. (b) Cherrier, M. M.; Borghesani, P. R.; Shelton, A. L.; Higano, C. S. Changes in neuronal activation patterns in response to androgen deprivation therapy: a pilot study. *BMC Cancer* **2010**, *10*, 1. (c) Whatcott, C. J.; Han, H.; Posner, R. G.; Hostetter, G.; Von Hoff, D. D. Targeting the Tumor Microenvironment in Cancer: Why Hyaluronidase Deserves a Second Look. *Cancer Discov.* **2011**, *1*, 291. (d) Yang, Z.; Qi, Y.; Lai, N.; Zhang, J.; Chen, Z.; Liu, M.; Zhang, W.; Luo, R.; Kang, S. Notch1 signaling in melanoma cells promoted tumor-induced immunosuppression via upregulation of TGF-β1. *J. Exp. Clin. Cancer Res.* **2018**, *37*, 1.

(8) (a) Benitez, A.; Yates, T. J.; Lopez, L. E.; Cerwinka, W. H.; Bakkar, A.; Lokeshwar, V. B. Targeting Hyaluronidase for Cancer Therapy: Antitumor Activity of Sulfated Hyaluronic Acid in Prostate Cancer Cells. *Cancer Res.* **2011**, *71*, 4085. (b) Kramer, M. W.; Escudero, D. O.; Lokeshwar, S. D.; Golshani, R.; Ekwenna, O. O.; Acosta, K.; Merseburger, A. S.; Soloway, M.; Lokeshwar, V. B. Association of hyaluronic acid family members (HAS1, HAS2, and HYAL-1) with bladder cancer diagnosis and prognosis. *Cancer* **2011**, *117*, 1197−1209.

(9) (a) Wang, Z.; Li, X.; Song, Y.; Li, L.; Shi, W.; Ma, H. An Upconversion Luminescence Nanoprobe for the Ultrasensitive Detection of Hyaluronidase. *Anal. Chem.* **2015**, *87*, 5816−5823. (b) Li, X.; Wu, T.; Fu, Y.; Ding, X.; Li, Z.; Zhu, G.; Fan, J. A high sensitivity background eliminated fluorescence sensing platform for hyaluronidase activity detection based on Si QDs/HA-δ-FeOOH nanoassembly. *Biosens. Bioelectron.* **2020**, *150*, 111928.

(10) Yang, W.; Ni, J.; Luo, F.; Weng, W.; Wei, Q.; Lin, Z.; Chen, G. Cationic Carbon Dots for Modification-Free Detection of Hyaluronidase via an Electrostatic-Controlled Ratiometric Fluorescence Assay. *Anal. Chem.* **2017**, *89*, 8384−8390.

(11) Liu, Q.; Yan, X.; Lai, Q.; Su, X. Bimetallic gold/silver nanoclusters-gold nanoparticles based fluorescent sensing platform via the inner filter effect for hyaluronidase activity detection. *Chemical* **2019**, *282*, 45−51.

(12) (a) Kim, J.-W.; Kim, J. H.; Chung, S. J.; Chung, B. H. An operationally simple colorimetric assay of hyaluronidase activity using cationic gold nanoparticles. *Analyst* **2009**, *134*, 1291−1293. (b) Shen, M.-Y.; Chao, C.-F.; Wu, Y.-J.; Wu, Y.-H.; Huang, C.-P.; Li, Y.-K. A design for fast and effective screening of hyaluronidase inhibitor using gold nanoparticles. *Sens. Actuators, B* **2013**, *181*, 605−610. (c) Nossier, A. I.; Eissa, S.; Ismail, M. F.; Hamdy, M. A.; Azzazy, H. M. E.-S. Direct detection of hyaluronidase in urine using cationic gold nanoparticles: A potential diagnostic test for bladder cancer. *Biosens. Bioelectron.* **2014**, *54*, 7−14.

(13) (a) Li, Z.; Tang, C.; Huang, D.; Qin, W.; Luo, F.; Wang, J.; Guo, L.; Qiu, B.; Lin, Z. Sensitive Hyaluronidase Biosensor Based on Target-Responsive Hydrogel Using Electronic Balance as Readout. *Anal. Chem.* **2019**, *91*, 11821−11826. (b) Dong, N.; Cai, Q.; Li, Z.; Xu, L.; Wu, H.; Lin, Z.; Qiu, B.; Li, C.; Lin, Z. Convenient

hyaluronidase biosensors based on the target-trigger enhancing of the permeability of a membrane using an electronic balance as a readout. *Analyst* **2021**, *146*, 3299−3304.
(14) (a) Dong, W.; Huang, Y. CeO2/C nanowire derived from a cerium(III) based organic framework as a peroxidase mimic for colorimetric sensing of hydrogen peroxide and for enzymatic sensing of glucose. *Microchim. Acta* **2019**, *187*, 11. (b) Li, Z.-X.; Zhang, J.-L.; Wang, J.; Luo, F.; Qiu, B.; Guo, L.-H.; Lin, Z.-Y. A Novel Enzyme-Responded Controlled Release Electrochemical Biosensor for Hyaluronidase Activity Detection. *J. Anal. Test.* **2021**, *5*, 69−75.
(15) Li, Z.; Chen, H.; Zhuo, Z.; Huang, D.; Luo, F.; Chen, L.; Wang, J.; Guo, L.; Qiu, B.; Lin, Z. Electrochemiluminescence biosensor for hyaluronidase activity detection and inhibitor assay based on the electrostatic interaction between hyaluronic acid and Ru(bpy)32+. *Chemical* **2018**, *275*, 409−414.
(16) Li, Z.; Zhang, J.; Chen, H.; Huang, X.; Huang, D.; Luo, F.; Wang, J.; Guo, L.; Qiu, B.; Lin, Z. Electrochemiluminescence Biosensor for Hyaluronidase Based on the Ru(bpy)32+ Doped SiO2 Nanoparticles Embedded in the Hydrogel Fabricated by Hyaluronic Acid and Polyethylenimine. *ACS Appl. Bio Mater.* **2020**, *3*, 1158−1164.
(17) (a) Qian, J.; Zhou, Z.; Cao, X.; Liu, S. Electrochemiluminescence immunosensor for ultrasensitive detection of biomarker using Ru(bpy)32+-encapsulated silica nanosphere labels. *Anal. Chim. Acta* **2010**, *665*, 32−38. (b) Zhang, L.; Dong, S. Electrogenerated Chemiluminescence Sensors Using Ru(bpy)32+ Doped in Silica Nanoparticles. *Anal. Chem.* **2006**, *78*, 5119−5123.
(18) Cheng, D.; Han, W.; Yang, K.; Song, Y.; Jiang, M.; Song, E. One-step facile synthesis of hyaluronic acid functionalized fluorescent gold nanoprobes sensitive to hyaluronidase in urine specimen from bladder cancer patients. *Talanta* **2014**, *130*, 408−414.
(19) Liu, S.; Zhao, N.; Cheng, Z.; Liu, H. Amino-functionalized green fluorescent carbon dots as surface energy transfer biosensors for hyaluronidase. *Nanoscale* **2015**, *7*, 6836−6842.
(20) Gu, W.; Yan, Y.; Zhang, C.; Ding, C.; Xian, Y. One-Step Synthesis of Water-Soluble MoS2 Quantum Dots via a Hydrothermal Method as a Fluorescent Probe for Hyaluronidase Detection. *ACS Appl. Mater. Interfaces* **2016**, *8*, 11272−11279.
(21) Hu, Q.; Zeng, F.; Wu, S. A ratiometric fluorescent probe for hyaluronidase detection via hyaluronan-induced formation of red-light emitting excimers. *Biosens. Bioelectron.* **2016**, *79*, 776−783.
(22) Li, X.; Zhou, Z.; Tang, Y.; Cheng Zhang, C.; Zheng, Y.; Gao, J.; Wang, Q. Modulation of assembly and disassembly of a new tetraphenylethene based nanosensor for highly selective detection of hyaluronidase. *Chemical* **2018**, *276*, 95−100.

https://doi.org/10.1021/acssensors.2c00801
ACS Sens. 2022, 7, 2012−2019